Density-functional Calculation of Structural Properties in Ionic and Semiconductor Crystals

Karin Schmalzl[1,2], Gernot Deinzer[3], Michael Malorny[1], and Dieter Strauch[1]

[1] Institut für Theoretische Physik, Universität Regensburg
93040 Regensburg, Germany
dieter.strauch@physik.uni-regensburg.de
[2] Institut Laue-Langevin, 38042 Grenoble Cedex 9, France
schmalzl@ill.fr
[3] Scuola Internazionale Superiore di Studi Avanzati (SISSA)
34014 Trieste, Italy
deinzer@sissa.it

Abstract. We compare the results of different ab-initio density-functional methods (WIEN97, VASP, ABINIT, PWSCF) and approximations for the electronic, structural, and dynamical properties of a variety of single crystals, namely the ionic conductors CaF_2, BaF_2, ZrO_2, and LaF_3, and the semiconductors CdS and CdSe. In particular, we have ported the PWSCF code to the Hitachi computer. These results are basic for the more extensive and current calculations of the static and lattice-dynamical properties of these systems as well as of systems like $ZrO_{2-\delta}$ and mixed-crystal systems like CdS_xSe_{1-x}. We also report preliminary neutron scattering data at various temperatures for the structure of LaF_3.

1 Introduction

The power of modern computer systems allows one to gain increasingly precise information about the properties of crystals. Even systems which were not tractable some years ago can be investigated now.

The increased computer power must be paralleled by permanent improvement and optimization of the employed programs. By the use of highly parallelized computing codes, we study various crystalline systems.

Even small displacements or even smallest nonlinearities influence the *dynamical* properties of ionic conductors or defect-stabilized structures. Since these properties depend on the ground-state *static* properties, a precise calculation of the latter is indispensable, and a test of the pseudopotentials and approximations used is thus essential.

For reasons of space limitation we restrict ourselves in the present report to a comparison of lattice-static properties of the pure systems as obtained

from various methods (even though we are actually interested in the lattice-dynamical properties of pure and defective systems): The ground-state properties (lattice constants and structural parameters) are determined from the (numerical) minimum of the total energy using the first-principles techniques mentioned below.

Our calculations are generally accompanied by neutron and synchrotron scattering experiments allowing a reliable check of the quality of our calculations and vice versa. In this connection we report preliminary data at 20, 150, and 300 K for the much-debated structure of LaF_3 from neutron-scattering experiments.

2 Methods

We employ ab-initio density-functional methods to compute the electronic, static, and harmonic lattice-dynamical properties. We have used various methods: The full-potential linearized augmented plane wave method is implemented in the WIEN97 code [1], the pseudopotential method is implemented in the ABINIT code [2], the VASP code [3], and in the PWSCF code [4]. The pseudopotential calculations have been done with Hartwigsen-Goedecker-Hutter pseudopotentials [5] (ABINIT) and ultrasoft pseudopotentials [6], [7] which are also available in the internet [8] (VASP and PWSCF). Within VASP also PAW pseudopotentials have been used [9]. Both, the local-density (LDA) and generalized-gradient (GGA) approximations have been applied.

Recently, the lesser-known PWSCF code has been ported to the Hitachi computer. It is a fully ab-initio code using a basis of plane waves and the pseudopotential method. The code is highly parallelized using MPI with a possible use of up to 128 processors. Two methods of parallelization have been implemented recently, namely that for the **k** points and that for the **R**- and **G**-space grids, where **R** and **G** are the direct and reciprocal lattice vectors. The **k**-point parallelization is very efficient. The speed is linear with the number of processors. The big disadvantage of this method is that all processors need the whole memory, and for that reason it is suitable only for not too large systems. The **R**-point and **G**-point parallelization does not scale as well as the **k**-point parallelization, but it reduces both, the memory of each node and the CPU time.

3 The systems

3.1 CaF_2 and BaF_2

The fluorine superionic conductors with the fluorite structure (CaF_2, BaF_2, and ZrO_2) and more complicated systems like LaF_3 display a conductivity, which can be comparable to that of a molten salt. These ionic conductors can

be applied in, e. g., fuel or galvanic cells or gas sensors. CaF_2 in particular with its large band gap has gained an importance as a material for lenses in the VUV nanolithography.

The origin of the ion transport mechanism is not completely clarified, but motional disorder in the fluorine sublattice and hopping over potential barriers is made responsible for it. The details of the conduction mechanism are believed to be different for the diverse classes of materials. In order to add to the understanding of this mechanism we have investigated the lattice statics and dynamics.

CaF_2 (as well as BaF_2) crystallizes in the fcc structure with one formula unit (three atoms) in the unit cell. It can be viewed as made up of tetrahedra and octahedra with the Ca atoms at the corners and with the F atoms at the centers of the tetrahedra. Figure 1 shows a cube containing four formula units; a complete octahedron is spanned by the Ca atoms on the face centers of the cube, while a tetrahedron is spanned by a Ca atom on a cube corner and the three adjacent Ca atoms on the face centers.

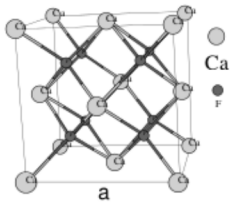

Fig. 1: Crystal structure of CaF_2: the fluorite structure.

3.2 ZrO_2 (zirconia)

ZrO_2 (zirconia), another ionic conductor, raised attention as a possible substitute for SiO_2 as the gate dielectric material in metal-oxide-semiconductors (MOS) devices. It is one of the most interesting and important materials in modern technologies. At low temperature ZrO_2 crystallizes in a monoclinic structure, which transforms with increasing temperature to a tetragonal and finally, above 2650 K, to a cubic fluorite structure, shown in Fig 1.

The transformation from tetragonal to monoclinic is rapid and is accompanied by a 3 to 5 percent volume increase that causes extensive cracking in the material. This behavior destroys the mechanical properties of fabricated components during cooling and makes pure zirconia useless for any structural or mechanical application.

For the technical applications, one is interested in the cubic phase: One mechanism to stabilize ZrO_2 is the addition of aliovalent oxides like CaO, MgO or Y_2O_3 [10]. It turns out that the mechanism is driven by the oxygen vacancies, the substitution of Ca, Mg or Y is just for charge neutrality [11]. Above a certain concentration of the dopant, the cubic phase is stable even at room temperature.

3.3 LaF_3

In contrast to the fluorite structures, the dynamics of LaF_3 has been discussed only rarely, probably because of the still debated structure: The La^{3+} ions are

in highly symmetric positions which alone would lead to a (pseudo) hexagonal unit cell with 2 formula units. Only small deviations of the F^- ions from high-symmetry positions lead to the actual cell with 6 formula units. Since the F^- ions carry much fewer electrons than the La^{3+} ions the positions of the F^- ions are difficult to determine from X-ray experiments. Different experiments have thus led to different crystal structures for LaF_3.

The two of the most often proposed structures, namely $P\bar{3}c1$ [12,13] and $P6_3cm$ [14] (the latter is of lower symmetry), differ only in small deviations of the F^- ion positions from those of the (ideal) hexagonal $P6_3/mmc$ symmetry. It seemed that the debate over these two structures had come to an end from the experimental point of view: LaF_3 and other tysonite-like compounds probably crystallize in a merohedral twinned structure, where each of the two twin domains has the $P\bar{3}c1$ symmetry, shown in Fig. 2. Ignoring the possible twinning leads to the $P6_3cm$ structure without a change of the lattice parameters. One claim is that the cause of twinning lies in structural defects [15]. Our own data reduction is still in progress.

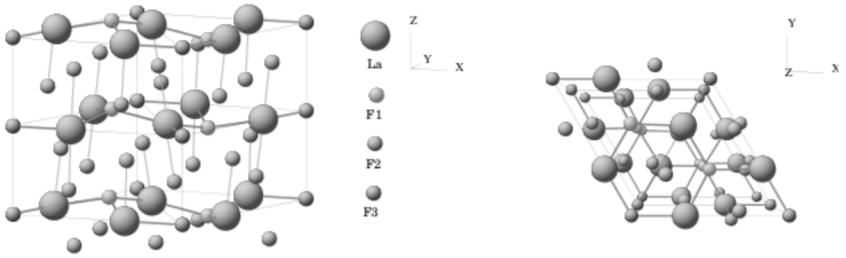

Fig. 2: The structure of LaF_3 ($P\bar{3}c1$ symmetry) (courtesy of A. Privalov) in side and top view. For a reproduction of this figure in colour, see Fig. 31 on page 476.

The theoretical results for LaF_3 are used in conjunction with the interpretation of our recent preliminary experimental neutron-scattering data between 20 K and room temperature.

Also in progress is the calculation of corresponding dynamical properties.

3.4 CdS and CdSe

The dynamics of mixed crystals is investigated in a project which combines theoretical and experimental techniques. The interest in mixed crystals has been renewed by the possible application of relaxor ferroelectrics like PZT ($PbZr_{1/2}Ti_{1/2}O_3$) or PMN ($PbMg_{1/3}Mn_{2/3}O_3$) as nonvolatile memories. CdS_xSe_{1-x} is taken as a simple model system for the structural, dynamical, and temperature dependent properties for the whole class of mixed semiconductors. Starting point for the statics and dynamics of the mixed-crystal

systems are the statics of the pure materials: At a later stage, the force constants of the mixed crystals will be taken from the pure materials (as a first approximation).

4 Results

4.1 Results for CaF_2 and BaF_2

A precise determination of the structure is needed as the starting point for all succeeding investigations of dynamical properties. In the case of CaF_2 an energy cut-off of 220 Ryd has been used within ABINIT and a cut-off of 80 Ryd within VASP for GGA and LDA. For comparison we have calculated static and dynamical properties of another ionic conductor, namely BaF_2. Within VASP, the calculations have been performed with PAW pseudopotentials in LDA with a cut-off of 80 Ryd and in GGA with 103 Ryd. In ABINIT a cut-off of 200 Ryd has been found to be necessary. In all cases a $4 \times 4 \times 4$ Monkhorst-Pack mesh has been used. A comparison of the obtained lattice constants is given in Table 1. Like in other cases, the lattice constant is underestimated in LDA, and overestimated in GGA. Hence phonon frequencies are generally overestimated in LDA and underestimated in GGA. The good agreement with the values obtained from the all-electron calculation (WIEN97) give us confidence in the used pseudopotentials.

Table 1: CaF_2 and BaF_2: Comparison of calculated lattice constant a (in Å) with experimental values from inelastic neutron scattering.

	CaF_2			BaF_2		
Method	LDA	GGA(PW)	GGA(PBE)	LDA	GGA(PW)	GGA(PBE)
WIEN97[1]	5.333	5.482	5.493	5.990	6.251	6.265
VASP[1]	5.173	5.44		6.094	6.279	
ABINIT(HGH)[1]	5.33			6.05		
PWSCF[1]			5.494			
ABINIT(TM)[2]	5.352		5.564			
CRYSTAL[3]	5.346	5.513				
Exp. (extrapol.)[1]	5.35					
Exp. (10 K)[1]	5.453					
Exp. (300 K)[1]	5.463					
Exp. (300 K)[4]	5.463			6.2		

[1]This work. [3]Ref. [18].
[2]Ref. [17] [4]Ref. [19].

As already pointed out elsewhere [16], CaF_2 shows an enormous shift of the lowest-frequency zone-boundary mode with increasing temperature. Especially this shift can be explained by volume expansion alone. Therefore a larger lattice constant, as obtained here in GGA, results in lower frequencies and thus in a larger disagreement with the experimental data taken at RT or below.

4.2 Results for ZrO_2

First of all, we have calculated the lattice parameters for the cubic and tetragonal structures of pure zirconia. Our calculations have been performed with ultra-soft pseudopotential within LDA. Cubic zirconia crystallizes in the CaF_2 structure. During the phase transition to the tetragonal phase, the c axis changes, and the pairs of atoms at the same x, y coordinates move along the c axis by a distance d. The resulting ground-state values are shown in Table 2.

For simulating the vacancies in cubic ZrO_2, we have used a supercell containing 96 atoms and have removed 4 oxygen atoms along the $(1, 1, 1)$ direction. This corresponds to 14.4 mol% Y_2O_3 which is sufficient to stabilize the cubic phase. The calculations for the ground-state structure are in good agreement with the results of Fabris *et al.* [11], who has used a self-consistent tight-binding model. Around the vacancies, the nearest Zr atoms move along the $(1, 1, 1)$ direction away from the site of the vacancy, while the nearest oxygen atoms move in the direction towards the vacancy.

With the new PWscf method and the possibility of using the Hitachi SR8000, linear response properties are also accessible even for a system as large as $ZrO_{2-\delta}$ with vacancies. The final goal is to determine the lattice dielectric properties of stabilized ZrO_2. The calculations of the dielectric constant and phonon frequencies are now in progress.

4.3 Results for LaF_3

Since the reported deviations of the F ions from highly symmetric positions are small we had originally hoped that we could save computer time assum-

Table 2: ZrO_2: Calculated ground-state lattice parameters in Å.

structure	a	c	d
cubic[1]	5.0201		
cubic[2]	5.0371		
tetr.[1]	5.0245	5.0999	0.0214
tetr.[2]	5.0299	5.1004	0.0221

[1]This work.
[2]Ref. [20].

ing a higher symmetric hexagonal structure ($P6_3/mmc$) and backfolding techniques. However the resulting dynamical properties are in disagreement with experimental data indicating that small lattice distortions may have a strong influence on the dynamical properties. A well grounded relaxed structure is thus necessary for reliable dynamical features concerning, e. g., defects or ionic conduction.

In contrast to the experimental situation, the structure is less clear from a theoretical point of view. We have made calculations for two different symmetries. A comparison of the obtained ground-state energies is given in Table 3. In the case of PWSCF our calculations have been performed with ultrasoft pseudopotentials with an energy cut-off fixed at 50 Ryd and a set of $2 \times 2 \times 2$ special points constructed after the method of Monkhorst and Pack. Within ABINIT we have used an energy cut-off of 220 Ryd and the same $2 \times 2 \times 2$ special-point mesh. For both, the hexagonal and the trigonal, symmetries, the resulting forces for the relaxed structures are less than $3 \cdot 10^{-3}$ Ryd/a_{Bohr} for each atom.

Table 3: LaF_3: Energies (in Ryd) of the relaxed $P\bar{3}c1$ and the $P6_3cm$ structure.

	ABINIT	PWSCF
$P\bar{3}c1$	-1256.6359	-1476.8959
$P6_3cm$	-1256.6332	-1476.8949

The calculations result in an energy difference for the the higher (tetragonal) $P\bar{3}c1$ symmetry only about 10^{-3} Ryd smaller than for the lower (hexagonal) $P6_3cm$ symmetry, see Table 3. From this difference, one is not able to decide which of the structures is energetically favored. To determine the actual structure of LaF_3 further calculations of important and possibly decisive physical properties like dielectric constants and phonon frequencies are necessary. This work as well as the reduction of neutron scattering data at 20, 150, and 300 K is in progress. Table 4 shows the partly preliminary results for the lattice constants in $P\bar{3}c1$ symmetry obtained with ab-initio methods and neutron scattering.

4.4 Results for CdS and CdSe

CdS and CdSe crystallize in the wurtzite structure as well as in the zinc-blende structure. Calculations by Wei and Zhang [24] show that CdS appears predominantly in the wurtzite structure at room temperature whereas CdSe exists in zinc-blende structure with the energy difference between the structures being very small.

Therefore, we have determined the lattice parameters of CdS and CdSe in the zinc-blende structure (with an old version on PWSCF) and in the wurtzite structure (with recent versions of ABINIT and PWSCF).

The pseudopotentials used in the former case have been generated with the LDA. For Cd the non-linear core correction (NLCC) has been applied to account for the role of the *d*-electrons. An energy cut-off of 16 Ryd has been enough to obtain converged values for the lattice constant a in either case. The Brillouin-zone integration has been performed using special $\mathbf{k}$ points forming a $4 \times 4 \times 4$ mesh. As a result, we have found values larger than retrieved from experiment in the case of CdS and smaller in the case of CdSe, see Table 5. All values lie within an error margin of 1%.

In the wurtzite case we have determined the structure with ABINIT by using pseudopotentials generated within LDA. As a cut-off energy we have chosen 60 Ryd and a $6 \times 6 \times 4$ $\mathbf{k}$-point mesh for the Brillouin-zone integration. As can be seen from Table 5 the calculated values for a and c are smaller than the experimental values and lie within an error margin of 1%.

The values determined with a recent version of PWSCF have been calculated using GGA-generated ultra-soft pseudopotentials in the case of Cd and S; the pseudopotential for Se was generated with the LDA. An energy cut-off of 40 Ryd has been used for CdS as well as CdSe, and a $6 \times 6 \times 4$ mesh has been applied. From Table 5 one finds that the calculated values are larger than the experimental ones in the case of CdS and smaller in the other case.

Table 4: LaF_3: Comparison of calculated lattice constants a and c (in Å) with experimental values from neutron diffraction for the $P\bar{3}c1$ symmetry.

Method	LDA		GGA(PBE)	
	a	c	a	c
VASP(PAW)[1]	7.026	7.201		
ABINIT(HGH)[2]	7.226	7.393		
CASTEP[3]			7.305	7.478
PWSCF[1]				
Exp. (295 K)[4]	7.20	7.37		
Exp. (300 K)[1]	7.186	7.355		
Exp. (150 K)[1]	7.178	7.341		
Exp. (20 K)[1]	7.171	7.336		
Exp. (300 K)[5]	7.188	7.359		

[1]This work.
[2]This work (preliminary).
[3]Ref. [21] (ultrasoft pseudopot.)
[4]Ref. [22]
[5]Ref. [23]

Table 5: CdS and CdSe: Comparison of calculated lattice constants a of the zinc-blende structure and a and c (in Å) of wurtizite structure with experimental values.

	Zinc-blende		Wurtzite			
	CdS	CdSe	CdS		CdSe	
Method	a	a	a	c	a	c
PWSCF[1]	5.869	6.072	4.185	6.829	4.249	6.951
ABINIT(HGH)[1]			4.122	6.699	4.290	6.972
Exp.[2]	5.821	6.054	4.136	6.714	4.300	7.011
Exp.[3]	5.83	6.084				

[1]This work. [2]Ref. [25] [3]Ref. [26]

The next step will be the calculation of the dynamical properties of these semiconductors to obtain a basis for the analysis of the mixed semiconductor CdS_xSe_{1-x} for which recent experimental synchrotron data exist. To achieve this goal super-cell methods will be applied which will require significant amounts of memory and calculation power.

4.5 Conclusion

Like in other cases, the lattice constants are underestimated in LDA, and overestimated in GGA. This has consequences on other physically relevant properties of the materials. For example, phonon frequencies are generally overestimated in LDA and underestimated in GGA. It is thus essential for all further calculations to have a good knowledge of the precision of the ground-state properties and of the sensitivity of selected dynamical properties on the static properties. Also, the ground-state properties should be compared with the experimental data at low temperatures where the total energy and the free energy differ least.

References

1. Blaha, P., Schwarz, K., Sorantin, P., Trickey, S. B. (1990): Full-potential, linearized augmented plane wave programs for crystalline systems. Comp. Phys. Comm. **59**, 399. (http://www.wien2k.at).
2. Gonze, X. (1997): First-principles responses of solids to atomic displacements and homogeneous electric fields: Implementation of a conjugate-gradient algorithm. Phys. Rev. B **55**, 10337. (http://www.abinit.org).
3. Kresse, G., Furthmüller, J. (1996): Efficient iterative schemes for ab initio total-energy calculations using a plane-wave basis set. Phys. Rev. B **54**, 11169. (http://cms.mpi.univie.ac.at/vasp).

4. Baroni, S., Dal Corso, A., de Gironcoli, S., Giannozzi, P.: http://www.pwscf.org.
5. Hartwigsen, C., Goedecker, S., Hutter, J. (1998): Relativistic separable dual-space Gaussian pseudopotentials from H to Rn. Phys. Rev. B **58**, 3641.
6. Vanderbilt, D. (1990): Phys. Rev. B **41**, 7892.
7. Kresse, G., Hafner, J. (1994): Norm-conserving and ultrasoft pseudopotentials for first-row and transition elements. J. Phys. Condens. Matter **6**, 8245.
8. A list of ultrasoft pseudopotentials can be found under the URL: http://www.physics.rutgers.edu/~dhv/uspp .
9. Kresse, G., Joubert, J. (1999): From ultrasoft pseudopotentials to the projector augmented wave method. Phys. Rev. B **59**, 1758.
10. Stapper, G., Bernasconi, M., Nicoloso, N., Parinello, M. (1999): Ab initio study of structural and electronic properties of yttria-stabilized cubic zirconia. Phys. Rev. B **59**, 797.
11. Fabris, S., Paxton, A. T., Finnis, M. (2002): Acta Materialia **50**, 5171.
12. Mansmann, M. (1965): Die Kristallstruktur von Lanthantrifluorid. Z. Kristallogr. **122**, 375.
13. Zalkin, A., Templeton, D. H. (1985): Refinement of the trigonal crystal structure of lanthanum trifluoride with neutron diffraction data. Acta Cryst. B **41**, 91.
14. Gregson, D., Catlow, C. R. A. (1983): The structure of LaF_3 - a single-crystal neutron diffraction study at room temperature. Acta Cryst. B **39**, 687.
15. Maksimov, B. A., Sirota, M. I., Galiulin, R. V., Sobolev, B. P. (1985): The crystal structure of PrF_3, and the twinning and symmetry of tysonite-like structures. Sov. Phys. Crystallogr. **30**, 164.
16. Schmalzl, K., Strauch, D., Schober, H. (2003): Lattice-dynamical and ground-state properties of CaF_2 studied by inelastic neutron scattering and density-functional methods. Phys. Rev. B **68**, 144301.
17. Verstraete, M., Gonze, X. (2003): First-principles calculation of the electronic, dielectric, and dynamical properties of CaF_2. Phys. Rev. B **68**, 195123.
18. Mérawa, M., Llunell, M., Orlando, R., Gelize-Duvignau, M., Dovesi, R. (2003): Structural, electronic and elastic properties of some fluoride crystals: an ab initio study. Chem. Phys. Lett. **368**, 7.
19. Wyckoff, R. W. G. (1963): Crystal Structures, Vol. 1, 2nd ed., Wiley, New York etc.
20. Zhao, X., Vanderbilt, D. (2002): Phonons and lattice dielectric properties of zirconia. Phys. Rev. B **65**, 75105.
21. Winkler, B., Knorr, K., Milman V. (2003): Prediction of the structure of LaF_3 at high pressures. J. Alloys. Comp. **349**, 111.
22. Belzner, A., Schulz, H. Heger, G. (1994): The thermal vibrations and the fluorine ionic conductivity in LaF_3. Z. Krist. **209**, 239.
23. Müller-Bunz, H., Schleid, T. (1999): $La_3F_3[Si_3O_9]$: Das erste Fluoridsilicat aus dem ternären System $LaF_3/La_2)_3/SiO_2$. Z. Anorg. Allg. Chem. **625**, 1377.
24. Wei, S. H., Zhang, S. B. (2000): Structure stability and carrier localization in CdX (X=S,Se,Te) semiconductors. Phys. Rev. B **62**, 6944.
25. Landolt-Börnstein (1982): Numerical Data and Functional Relationships in Science and Technology, edited by O. Madelung, Springer-Verlag, Berlin, Vol. 17b.
26. Abrikosov, N. Kh., Bankina, V. B., Poretskaya, L. V., Shelimova, L. E., Skudnova, E. V. (1969): Semiconducting II-IV, IV-VI, and V-VI Compounds. Plenum, New York, p. 2.

Planar Helium under Electromagnetic Driving

Javier Madroñero and Andreas Buchleitner

Max-Planck-Institut für Physik komplexer Systeme
Nöthnitzer Str. 38, 01187 Dresden, Germany
jma@mpipks-dresden.mpg.de, abu@mpipks-dresden.mpg.de

Abstract. We report on the successful numerical implementation of an original method for the accurate quantum treatment of helium under electromagnetic driving. Our approach is the first to allow for a description of the highly complex quantum dynamics of this system, in the entire non-relativistic parameter regime, i.e., it provides full spectral and dynamical information on the ionization of the atomic ground state by optical fields, as well as on the dynamics of doubly excited Rydberg states under radiofrequency driving. As a by-product, the non-trivial role of the dimension of configuration space for the field-free dynamics of doubly excited helium is elucidated.

1 Introduction

The quantum mechanical treatment of the helium atom goes back to the early days of quantum mechanics: Einstein was the first [1] to realize that the then available quantization schemes which had been applied successfully in the analysis of the atomic spectra of one electron atoms would be inoperational for this microscopic realization of the gravitational three body problem: As first noticed by Poincaré, the classical dynamics of the latter is nonintegrable, and this remains true when gravitational forces are substituted by attractive and repulsive Coulomb forces, such as to define the three body Coulomb problem. Indeed, the electron-electron interaction term in the Hamiltonian of the unperturbed helium atom – which otherwise is just the sum of two hydrogen Hamiltonians with amended nuclear charge – renders the two-electron dynamics in general irregular or chaotic, with only rather small domains of the classical phase space occupied by regular, i.e., integrable, motion. On the quantum level, the loss of integrability is tantamount to the (at least partial) destruction of good quantum numbers, and leads to an abundance of intriguing and surprising effects, such as the autoionization of doubly excited states [2], Ericson fluctuations in the photocrossection at high excitation energies [3],